ISSN (e): 2250 – 3005 || Volume, 07 || Issue, 06|| June – 2017 ||
International Journal of Computational Engineering Research (IJCER)

Boundary Layer Flow Of MHD Tangent Hyperbolic Fluid Past A Vertical Plate In The Presence Of Thermal Dispersion Using Spectral Relaxation Method

Uma maheswara rao K[1], G.Koteswara rao[2]
[1]Department of Mathematics, Hyderabad Institute of Technology and management, Gowdavelly village, Rangareddy district, Hyderabad, Telangana 501401
[2]Department of Mathematics, Acharya Nagarjuna University,Guntur522510

ABSTRACT

In this present study, a numerical investigation has been carried out to discuss the steady, two dimensional flow of heat and mass transfer of electrically conducting tangent hyperbolic fluid in the presence of thermal dispersion. The tangent hyperbolic fluid is a four constant fluid model capable of describing shear thinning effects. The apparent viscosity for the proposed varies gradually between zero shear rate and shear rate tending to infinity. The flow is induced by a stretching surface. The solutions of the transformed nonlinear equations have been obtained by using Spectral Relaxation Method (SRM) and the results are validated by comparison with numerical approximations obtained using the Matlab in-built boundary value problem solver bvp4c, and with existing results available in literature. The results are presented graphically and discussed for various resulting parameters. Wessenberg number increases the thickness of the fluid, so velocity profiles decrease with an increase in We . htermophoresis effect significantly increases the thermal and concentration boundary layer thickness. Both local Nusselt numbers and local Sherwood numbers give same behavior for Weissenberg number. Thermal dispersion strongly influenced the temperature profile.

Keywords: *Stretching sheet, tangent hyperbolic fluid, nanofluid, SRM.*

I. INTRODUCTION

During the past many years, number of researchers has worked on non-Newtonian fluids. Wang [1] analyzed non- Newtonian fluids for mixed convection heat transfer from a vertical plate. Xu and Jan Liao [2] studied the laminar boundary layer flow and heat and mass transfer analysis of non-Newtonian fluids past a stretching flat sheet. Xu et al. [3] have presented the series solutions of unsteady boundary layer flows of non-Newtonian fluids near a forward stagnation point. In another study, Megahed [4] investigated the boundary layer flow and heat transfer of a non-Newtonian power – law fluid over a non-linearly stretching vertical surface with heat fluid and thermal radiation. Abel et al. [5] studied the boundary layer flow and heat transfer in a power law fluid through a stretching sheet with variable thermal conductivity and non-uniform effects. Bilal Ashraf et al. [6] discussed the mixed convection flow of Jeffrey nanofluid over a radially stretching surface with thermal radiation effect. Wei and Al-Ashhab [7] have studied the boundary layer flow of power law non-Newtonian fluids with a novel boundary condition. The heat transfer mechanism and the constitutive models for energy boundary layer in power law fluids have been discussed by Zheng and Zhang [8]. An analytical solution for boundary layer flow and heat transfer of non-Newtonian fluids in a porous media on an isothermal semi-infinite plate has been studied by Wang and Tu [9]. Hady [10] has analyzed the influence of laminar mixed convection flow of non-Newtonian fluids along a horizontal plate for uniform wall temperature. Effects of boundary induced stream wise pressure gradients on laminar forced convection flow of heat transfer to non-Newtonian fluids from a horizontal plate have been examined by Gorla [11]. Mostafa [12] presented the slip effect on non-Newtonian power law fluid past a continuously moving surface with suction using shooting method.

An important branch of the non-Newtonian fluid models is the hyperbolic tangent fluid model. The hyperbolic tangent fluid is used extensively for different laboratory experiments. Friedman et al. [13] have used the hyperbolic tangent fluid model for large-scale magneto-rheological fluid damper coils. Nadeem and Akram [14] jointly published a paper on peristaltic transport of a hyperbolic tangent fluid model in an asymmetric channel. In another paper Nadeem and Akram [15] have presented the effects of partial slip on the peristaltic transport of a hyperbolic tangent fluid model in an asymmetric channel. Natural convection boundary layer flow of a hyperbolic tangent fluid flowing past a vertical exponential circular cylinder with heat transfer analysis has been studied by Naseer et al. [16].

All the above investigations are restricted to MHD flow and mass transfer problems. Analysis of heat and mass transfer of a viscoelastic, electrically conducting fluid past a continuous stretching sheet was investigated by Kelly et al. [17]. Vajravelu et al. [18] investigated the effects of velocity slip, temperature and concentration jump conditions on MHD peristaltic transport of a Carreau fluid in a non-uniform channel. Jayachandra babu and Sandeep [19] both are investigated the effects of cross diffusion and MHD on non Newtonian fluid flow over a slandering stretching sheet. Effect of MHD and heat transfer effects on a boundary layer flow of power law non-Newtonian nonofluid over a vertical stretching sheet is studied by Ferdows and Hamad [20]. Satyanarayana and Harish Babu [21] studied the effects of chemical reaction, thermal radiation and MHD on heat and mass transfer of a Jeffrey fluid over s stretching sheet. They concluded that effect of magnetic fields significantly decelerate the velocity of the flow field to an appropriate amount through boundary layer. Kasim and Mohammad [22] studied the effects of thermal stratification, heat source, MHD, Hall current and chemical reaction on heat and mass transfer over an unsteady stretching surface. Rushi Kumar [23] investigated the effects of magnetohydrodynamic and velocity slips on a flow, heat and mass transfer over a stretching sheet. Soret and dufour effects on MHD convective radiative heat and mass transfer of nanofluids over a vertical non-linear stretching/shrinking sheet is investigated by Pal et al. [24].Similarity solution of the boundary layer equations describing heat and flow in a non-Newtonian power law fluid by a continuously moving surface with a parallel free stream subject to MHD have been examined numerically by Kumari and Nath [25]. Akbar et al. [26] investigated the boundary layer flow of magnetohydrodynamic tangent hyperbolic fluid past a stretching sheet with the help of fourth-fifth order Runge-Kutta Fehlberg method. They came to the conclusion that Weissenberg number significantly decreases the velocity profile. Salahuddin et al. [27] studied the tangent hyperbolic fluid with exponentially varying viscosity in the presence of transverse magnetic field.

Dispersion mechanisms in porous media have shown to be more pronounced when compared to those in pure fluids. This may be attributed to the additional effect caused by the complex tortuous passages of porous media and to the fact that they depend on the average velocity of the fluid within the pores. On the other hand, thermal and solutal-dispersion effects are more important when the inertial effects are prevalent. Several studies on hydrodynamic dispersion in porous media have been reported by Bear [28]. Analogously to hydrodynamic dispersion, thermal dispersion has also been postulated to depend on the structures of the given porous media and the average velocity (over a representative elementary volume) of the saturating fluid. A linear dispersion model introduced by Georgiadis and Catton [29] was assumed for the case of free convection in a horizontal layer heated from below. An analysis of thermal-dispersion effects on natural convection along a heated, vertical plate in porous media was presented by Hong and Tien [30]. Double dispersion and chemical reaction effects on non-Darcy free convection heat and mass transfer is studied by El-Amin et al. [31].

The above cited articles in the literature explicates the flow and the heat and mass transfer characteristics of different working fluids in stretching sheet It can be noticed that consideration tangent hyperbolic fluid as working fluid has greater interest in practical applications in science and engineering. As a trial attempt, the authors intend to provide the knowledge of the effects of the steady, two dimensional flow of heat and mass transfer of magnetic tangent hyperbolic fluid over a stretching sheet in the presence of thermal dispersion.

Mathematical Formulation

Consider the problem of two-dimensional flow of steady incompressible and electrically conducting tangent hyperbolic fluid over a wall coinciding with plane $y = 0$, the flow is being confined to $y > 0$. the flow is generated due to the linear stretching.

The constitutive equation of tangent hyperbolic fluid is [26]:

$$\bar{\tau} = \left[\mu_\infty + (\mu_0 + \mu_\infty)\tanh\left(\Gamma\bar{\dot{\gamma}}\right)\right]\bar{\dot{\gamma}} \tag{1}$$

In which, $\bar{\tau}$ is the extra stress tensor, μ_∞ is the infinite shear rate viscosity, μ_0 is the zero shear rate viscosity, Γ is the time dependent material constrant, n is the power law index i.e flow behavior index and $\bar{\dot{\gamma}}$ is defined as

$$\bar{\dot{\gamma}} = \sqrt{\frac{1}{2}\sum_i\sum_j \bar{\dot{\gamma}}_{ij}\bar{\dot{\gamma}}_{ji}} = \sqrt{\frac{1}{2}\Pi} \tag{2}$$

Where $\Pi = \frac{1}{2}tr\left(gradV + (gradV)^T\right)^2$. We consider equation (1), for the case of $\mu_\infty = 0$ because it is not possible to discuss the problem for the infinite shear rate viscosity and since we are considering tangent hyperbolic fluid that describing shear thinning effects so $\Gamma\bar{\dot{\gamma}} < 1$. Then equation (1) takes the form

$$\bar{\tau} = \mu_0\left[\left(\Gamma\bar{\dot{\gamma}}\right)^n\right]\bar{\dot{\gamma}} = \mu_0\left[\left(1 + \Gamma\bar{\dot{\gamma}} - 1\right)^n\right]\bar{\dot{\gamma}} = \mu_0\left[\left(1 + n(\Gamma\bar{\dot{\gamma}} - 1)\right)\right]\bar{\dot{\gamma}} \tag{3}$$

The external force f may be written as follows:

$$f = J \times B \tag{4}$$

where $J = \sigma_0 (E + V \times B)$ is the current density and $B = (0, B_0)$ is the transverse uniform magnetic field applied to the fluid layer. The symbols σ_0 and E are the electric conductivity and the electric field, respectively. The external electric field is assumed to be zero and under the condition that magnetic Reynolds number is small the induced magnetic field is negligible compared with the applied field. Accordingly, the Hall effect is neglected.

The boundary layer temperature and concentration are T and C respectively. The ambient fluid temperature and concentration are T_∞ and C_∞ respectively. At the surface, both the fluid and the sheet are kept at a constant temperature T_w where $T_w > T_\infty$ is for a heated stretching surface and $T_w < T_\infty$ corresponds to a cooled surface. The continuity, momentum, energy and species equations for the tangent hyperbolic fluid after applying the boundary layer approximations can be expressed as:

$$\frac{\partial u}{\partial x} + \frac{\partial v}{\partial y} = 0 \tag{5}$$

$$u\frac{\partial u}{\partial x} + v\frac{\partial u}{\partial y} = \upsilon(1-n)\frac{\partial^2 u}{\partial y^2} + \sqrt{2}\upsilon n\Gamma\left(\frac{\partial u}{\partial y}\right)\frac{\partial^2 u}{\partial y^2} - \frac{\sigma B_0^2}{\rho}u \tag{6}$$

$$u\frac{\partial T}{\partial x} + v\frac{\partial T}{\partial y} = \frac{\partial}{\partial y}\left(\alpha_e \frac{\partial T}{\partial y}\right) \tag{7}$$

$$u\frac{\partial C}{\partial x} + v\frac{\partial C}{\partial y} = D\frac{\partial^2 C}{\partial y^2} \tag{8}$$

Boundary conditions are

$$y = 0 : u = u_w = ax, v = 0, T = T_w, C = C_w \tag{9}$$

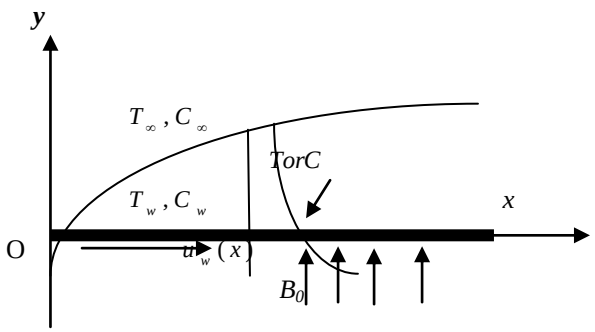

Figure A: Schematic diagram of the problem

$$y \to \infty : u \to 0, T \to T_\infty, C \to C_\infty \tag{10}$$

We are interested in similarity solution of the above boundary value problem; therefore, we introduce the following similarity transformations

$$u = axf'(\eta), v = -\sqrt{a\upsilon}\, f(\eta), \eta = \sqrt{\frac{a}{\upsilon}}y, \theta(\eta) = \frac{T - T_\infty}{T_w - T_\infty}, \phi(\eta) = \frac{C - C_\infty}{C_w - C_\infty} \tag{11}$$

Making use of transformations (11), Equations (5)-(10) take the form

$$(1-n)f''' + ff'' - f'^2 + nWe\, f'''(f'') - Mf' = 0 \tag{12}$$

$$\theta''(1 + Ds\, f') + Ds\, \theta' f'' + \Pr\, f\theta' = 0 \tag{13}$$

$$\phi'' + Scf\, \phi' = 0 \tag{14}$$

The transformed boundary conditions

$$f(0) = 0,\ f'(0) = 1, \theta(0) = 1, \phi(0) = 1 \tag{15}$$

$$f'(\infty) = 0, \theta(\infty) = 0, \phi(\infty) = 0 \tag{16}$$

The non-dimensional constants in Equations (12)-(14) are the Weissenberg number We , the Prandtl number $\Pr$, Hartmann number M , thermal dispersion parameter Ds and the Schmidt number Sc . They are, respectively, defined as:

$$We = \frac{\sqrt{2a}u_w\Gamma}{\sqrt{\upsilon}}, \Pr = \frac{\upsilon}{\alpha}, M = \frac{\sigma B_0^2}{\rho a}, Ds = \frac{\gamma d u_w}{\alpha_m}, Sc = \frac{\alpha}{D} \tag{17}$$

These parameters, respectively, characterize the surface drag, wall heat and mass transfer rates. The shearing stress at the surface of the wall τ_w is given by:

$$\tau_w = \left[(1-n)\frac{\partial u}{\partial y} + \frac{n\Gamma}{\sqrt{2}}\left(\frac{\partial u}{\partial y}\right)^2 \right]_{y=0} \tag{18}$$

where μ is the coefficient of viscosity. The skin friction coefficient is defined as:

$$C_f = \frac{\tau_w}{\rho u_w^2} \tag{19}$$

and using Equation (17) in (18) we obtain:

$$C_{fx}\,\mathrm{Re}_x^{1/2} = \left[(1-n) f''(0) + \frac{n}{2} We\,(f''(0))^2 \right] \tag{20}$$

The heat transfer rate at the surface flux at the wall is given by:

$$q_w = -k\left(\frac{\partial T}{\partial y}\right)_{y=0} \tag{21}$$

where k is the thermal conductivity of the nanofluid. The Nusselt number is defined as:

$$Nu_x = \frac{x}{k}\frac{q_w}{T_w - T_\infty} \tag{22}$$

Using Equation (21) in (22) the dimensionless wall heat transfer rate is obtained as below:

$$\frac{Nu_x}{\mathrm{Re}_x^{1/2}} = -\theta'(0) \tag{23}$$

The mass flux at the surface of the wall is given by:

$$J_w = -D\left(\frac{\partial C}{\partial y}\right)_{y=0} \tag{24}$$

and the Sherwood is defined as:

$$Sh_x = \frac{x}{D}\frac{J_w}{C_w - C_\infty} \tag{25}$$

Using Equation (24) in (25) the dimensionless wall mass transfer rate is obtained as:

$$\frac{Sh_x}{\mathrm{Re}_x^{1/2}} = -\phi'(0) \tag{26}$$

In Equations (20), (23) and (26), Re_x represents the local Reynolds number defined by

$$\mathrm{Re}_x = \frac{x u_w(x)}{\upsilon}$$

Solution of the Problem:

In order to solve the equations (12)-(14) subject to the boundary conditions (15) and (16) the Spectral Relaxation Method (SRM) suggested by Motsa and Makukula [32] and Kameswaran et al. [33] is used. The method uses the Gauss- Seidel approach to decouple the system of equations. In the framework of SRM method

the iteration scheme is obtained as $f'_{r+1} = p_r,\ f_{r+1}(0) = 0$

(27)

$$p''_{r+1} + (nWe\ p' - n)p'_{r+1} + (f_{r+1})p_{r+1} - Mp_{r+1} = p_r^2 \quad (28)$$

$$\theta''_{r+1}(1 + Dsp_{r+1}) + (Ds\ p'_{r+1} + \Pr\ f_{r+1})\theta'_{r+1} = 0 \quad (29)$$

$$\phi''_{r+1} + Sc(f_{r+1})\phi'_{r+1} = 0 \quad (30)$$

The boundary conditions for the above iteration scheme are

$$p_{r+1}(0) = 1, \theta_{r+1}(0) = 1, \phi_{r+1}(0) = 1 \quad (31)$$

$$p_{r+1}(\infty) = 0, \theta_{r+1}(\infty) = 0, \phi_{r+1}(\infty) = 0 \quad (32)$$

In order to solve the decoupled equations (27) - (30), we use the Chebyshev spectral collocation method. The computational domain [0, *L*] is transformed to the interval [-1, 1] using $\eta = L(\xi + 1)/2$ on which the spectral method is implemented. Here L is used to invoke the boundary conditions at ∞. The basic idea behind the spectral collocation method is the introduction of a differentiation matrix $\mathcal{D}$ which is used to approximate the derivatives of the unknown variables at the collocation points as the matrix vector product of the form

$$\frac{\partial f_{r+1}}{\partial \eta} = \sum_{k=0}^{\overline{N}} D_{lk} f_r(\xi_k) = Df_r, l = 0,1,2,..... \overline{N} \quad (33)$$

where $\overline{N} + 1$ is the number of collocation points (grid points), D = 2$\mathcal{D}$/L, and $f = \left[f(\xi_0), f(\xi_1), f(\xi_2),..... .f(\xi_{\overline{N}})\right]^T$ is the vector function at the collocation points. Higher-order derivatives are obtained as powers of D, that is,

$$f_r^{(p)} = D^p f_r \quad (34)$$

where p is the order of the derivative. Applying the spectral method to equations (27)- (30), we obtain

$$A_1 f_{r+1} = B_1,\ f_{r+1}(\xi_{\overline{N}}) = 0 \quad (35)$$

$$A_2 p_{r+1} = B_2,\ p_{r+1}(\xi_{\overline{N}}) = 1,\ p_{r+1}(\xi_0) = 0 \quad (36)$$

$$A_3\theta_{r+1} = B_3, \theta_{r+1}(\xi_{\overline{N}}) = 1, \theta_{r+1}(\xi_0) = 0 \quad (37)$$

$$A_4\phi_{r+1} = B_4, \phi_{r+1}(\xi_{\overline{N}}) = 1, \phi_{r+1}(\xi_0) = 0 \quad (38)$$

where,

$$A_1 = D, B_1 = p_r \quad (39)$$

$$A_2 = D^2 + diag\ (nWe\ p'_{r+1} - n)D^2 + diag\ (f_{r+1})D - MI\ , B_2 = p_r^2 \quad (40)$$

$$A_3 = diag\ (1 + Dsp_{r+1})D^2 + diag\ (\Pr\ f_{r+1} + Ds\ p'_{r+1})D, B_3 = 0 \quad (41)$$

$$A_4 = D^2 + diag\ (Scf_{r+1})D, B_4 = 0 \quad (42)$$

In equations (39)-(42), I is an identity matrix and diag[ ] is a diagonal matrix, all of size $(\overline{N} + 1) \times (\overline{N} + 1)$ where $\overline{N}$ is the number of grid points, f, p, θ and ϕ are the values of the functions f, p, θ and ϕ, respectively, when evaluated at the grid points and the subscript r denotes the iteration number. The initial guesses to start the SRM scheme for equations (27)-(32) are chosen as

$$f_0(\eta) = 1 - e^{-\eta}, p_0(\eta) = e^{-\eta}, \theta_0(\eta) = e^{-\eta}, \phi_0(\eta) = e^{-\eta} \quad (43)$$

which are randomly chosen functions that satisfy the boundary conditions. The iteration is repeated until convergence is achieved. The convergence of the SRM scheme is defined in terms of the infinity norm as

$$Er = Max\left(\left\|f_{r+1} - f_r\right\|, \left\|p_{r+1} - p_r\right\|, \left\|\theta_{r+1} - \theta_r\right\|, \left\|\phi_{r+1} - \phi_r\right\|\right) \quad (44)$$

Accuracy of the scheme is established by increasing the number of collocation points $\overline{N}$ until the solutions are consistent and further increases do not change the value of the solutions.

Validation of Results:

The accuracy and robustness of the method have been checked by comparing the SRM results and bvp4c results for various values of power law index parameter n, Weissenberg number We, Hartmann number *M*, Prandtl number *Pr*, thermal dispersion parameter *Ds* and Schmidt number Sc which are given in tabular form in Tables 1 to 4. It is clearly seen that both results are in good agreement. It is relevant to mention here that bvp4c is an in-

built ODE solver in Matlab. In order to further establish the accuracy of our numerical computations, we have also compared the values of magnitude of the skin friction coefficient C_{fx} obtained by Akber et al. [26], respectively with the respective values calculated by the SRM technique. This comparison is presented in Tables 4 and it has been observed that our results are in full agreement with the results obtained by Akber et al. [26].

II. RESULTS AND DISCUSSION

We have studied steady heat and mass transfer in a tangent hyperbolic fluid past a stretching sheet. Nanofluid has been considered for the present investigation. The tangent hyperbolic fluid is a four constant fluid model capable of describing shear thinning effects. The apparent viscosity for the proposed varies gradually between zero shear rate and shear rate tends to infinity. The nonlinear coupled ordinary differential equations (12)-(14) subject to the boundary conditions (15)-(16) have been solved numerically using spectral relaxation method. We determine through numerical experimentation that $\eta_\infty = 15$ with the grid points $\overline{N} = 100$, give sufficient accuracy for the spectral relaxation method. To determine the convergence, accuracy and general validity of the SRM method, the results were compared with the Matlab bvp4c results for selected values of the governing physical parameters.

Figs. 1-11 illustrate the behavior of emerging parameters such of power law index parameter n , Weissenberg number We , Hartmann number *M*, Prandtl number *Pr*, thermal dispersion parameter *Ds* and Schmidt number Sc on velocity profile $f'(\eta)$, temperature profile $\theta(\eta)$ and concentration profile $\phi(\eta)$. Figs 1-3 depict the variation of unsteadiness parameter S on velocity profile $f'(\eta)$, temperature profile $\theta(\eta)$ and mass friction function $\phi(\eta)$. Figures 1-3 depict the behavior of power law index n on velocity, temperature and concentration profiles. It is observed that velocity profiles decrease with an increase in n. But boundary layer thickness increases. From the graphs 2 & 3, it is noticed that temperature and concentration profiles increases with an increase in n and also thermal and concentration boundary layer thickness increases. The dimensionless velocity $f'(\eta)$, temperature $\theta(\eta)$ and concentration $\phi(\eta)$ profiles for different values of Weissenberg number We are plotted in figures 4-6, respectively. Weissenberg number is the ratio of the relaxation time of the fluid and a specific process time. In simple steady shear, the Weissenberg number is defined as the shear rate times and the relaxation time. It increases the thickness of the fluid, so velocity profiles decrease with an increase in We . Also boundary layer thickness decreases for increasing values of We (see fig.4). From the graphs 5 & 6, it is clearly observed that temperature and concentration of the fluid increase with a rise in We . But boundary layer thickness for temperature and concentration increases with an increase in We . Figure 7 and 8 shows the influence of Hartmann number *M* on velocity, temperature and concentration profiles. Hartmann number is the ratio of electromagnetic force to the viscous force. Consequently, Hartmann numbers resist the fluid flow. It is seen from figure 7 that velocity profile decreases with the increasing values of *M* and the boundary layer thickness increases. It is also analyzed that *M* is perpendicular to the stretching sheet so for higher values of *M* it decelerates the velocity and raise the boundary layer thickness. From figures 8 and 9, that temperature and concentration profiles increases with an increase in *M* and corresponding boundary layers also increases. Figures 10 and 11 are graphed for the effects of increasing values of the Prandtl number *Pr* on temperature and concentration profiles. Physically, the Prandtl number is a dimensionless number which is the ratio of momentum diffusivity (Kinematic viscosity) to thermal diffusivity. Increasing the values of the Prandtl number means that momentum diffusivity dominates thermal diffusivity. Thus, the temperature and concentration decreases with an increase in Prandtl number values. Figure 12 shows that the effects of thermal dispersion on temperature profile. From the sketch, an increase in the thermal dispersion effect increases the thermal boundary layer thickness i.e. thermal dispersion enhances the transport of heat along the normal direction to the wall as compared with the case where dispersion is neglected (i.e. *Ds* = 0). In general, this for may be useful in showing that, the use of fluid medium with better heat dispersion properties may be result in better heat transfer characteristics that may be required in many industrial applications (like those concerned with packed bed reactors, nuclear waste disposal, etc.). Figure 13 shows the behavior of concentration profile for Schmidt number Sc . It is observed that concentration profiles decreases for higher values of *Sc*. Consequently, boundary layer thickness decreases indefinitely with an increase in *Sc*.

Table 1 contains the boundary derivatives for velocity profile at the surface of the stretching sheet that corresponds to shin friction coefficient C_{fx} calculated for different values of the power law index n , Weissenberg number We and Hartmann number *M*. From the data in table 1, it is noticed that increase in both power law index n and Weissenberg number We decreases the magnitude of skin friction coefficient C_{fx} , but

skin friction coefficient significantly increases with an increase in *M*. Table 2 is included to check the behavior of derivative for temperature profile that also predict the local Nusselt number Nu_x tabulated for different values of power law index n, Weissenberg number We, Hartmann number *M*, thermal dispersion parameter *Ds* and Prandtl number Pr. From the entries in table 2, it is observed that with increases in Prandtl number *Pr*, local Nusselt number Nu_x increases, whereas local Nusselt number Nu_x values decrease for increase in power law index n, Weissenberg number We, Hartmann number M and thermal dispersion parameter Ds. Table 3 contains the derivative for concentration profile that also gives the behavior of local Sherwood number Sh_x for different values of power law index n, Weissenberg number We, Hartmann number *M*, Prandtl number Pr and Schmidt number Sc. From the data in table 3, it is observed that with the increase in power law index n, Weissenberg number We, and Hartmann number Nt, local Sherwood number Sh_x decreases, while increase in Prandtl number *Pr*, Schmidt number Sc, decrease the local Sherwood number Sh_x.

III. CONCLUSIONS

In this study we have presented the heat and mass transfer in magnetohydrodynamic tangent hyperbolic fluid flow over stretching sheet in the presence of thermal dispersion. The main results of present analysis are listed below

- Weissenberg number and power law index increase the thickness of the fluid, so velocity profile decreases with an increase in We and n.
- Weissenberg number and power law index increase the thickness for the thermal and concentration boundary layers, so the temperature and concentration profiles increases with an increase in We and n.
- The thermal dispersion parameter has a strong influence over the temperature profiles.
- Effect of Hartmann number M for local Nusselt number and Sherwood numbers are similar. Since M causes to reduce the local Nusselt number and Sherwood numbers.
- The effect of *Pr* gives the same behavior for both local Nusselt number and Sherwood numbers. Since *Pr* causes to enhances the local Nusselt number and Sherwood numbers.

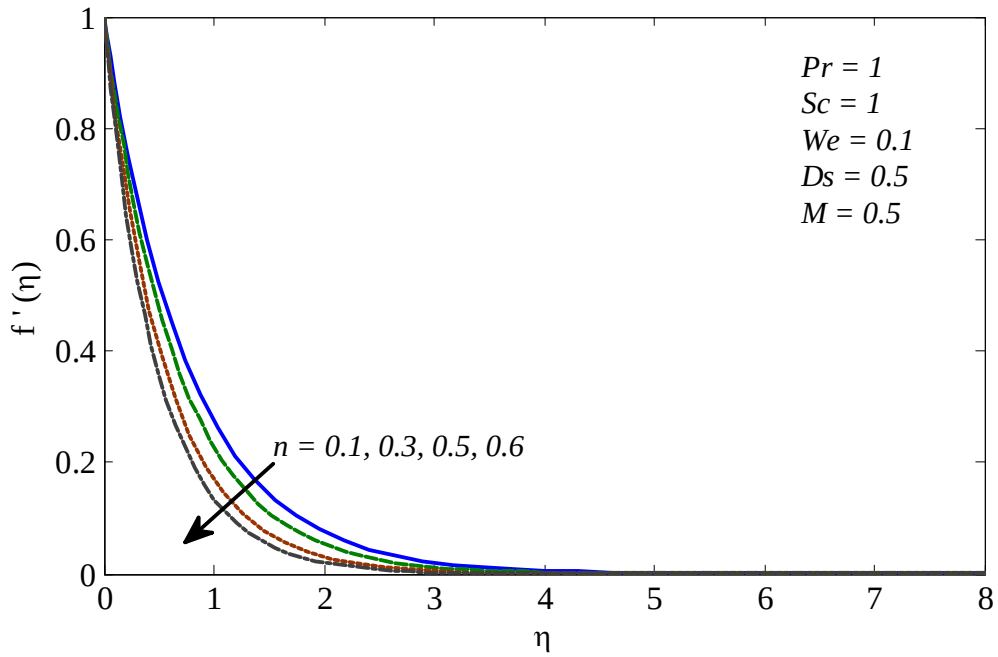

Figure 1: Graph of SRM solutions for velocity profile $f'(\eta)$ for different values of n

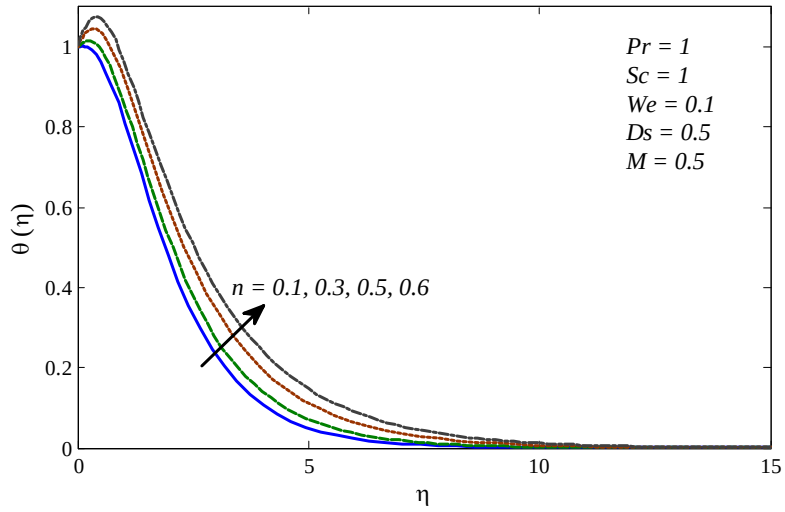

Figure 2: Graph of SRM solutions for temperature profile $\theta(\eta)$ for different values of n

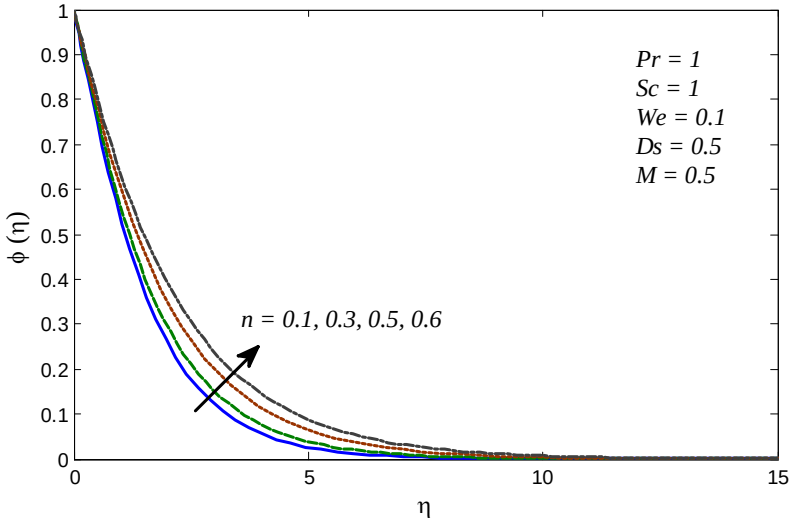

Figure 3: Graph of SRM solutions for concentration profile $\phi(\eta)$ for different values of n

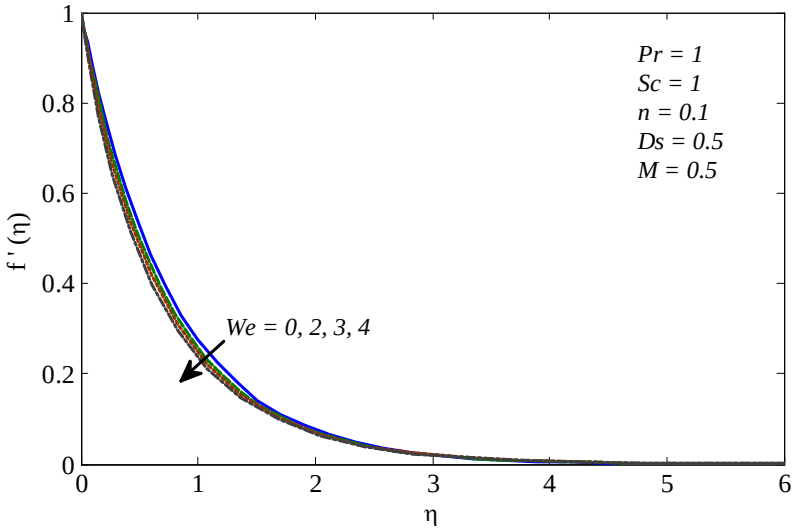

Figure 4: Graph of SRM solutions for velocity profile $f'(\eta)$ for different values of We

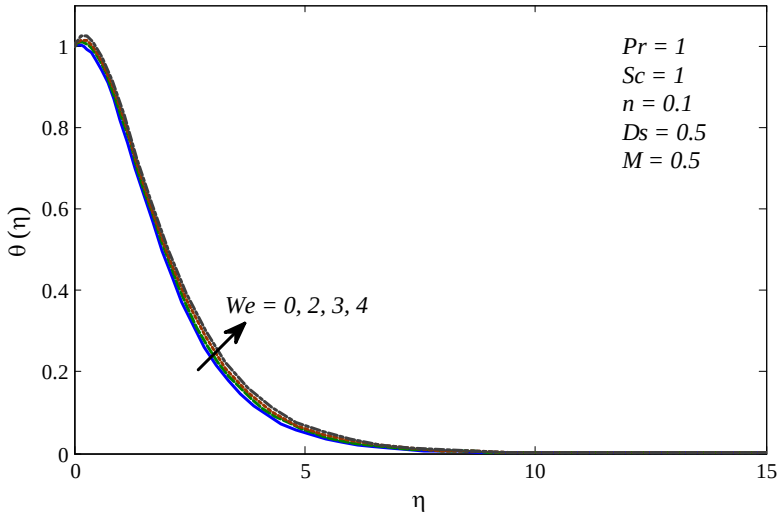

Figure 5: Graph of SRM solutions for temperature profile $\theta(\eta)$ for different values of *We*

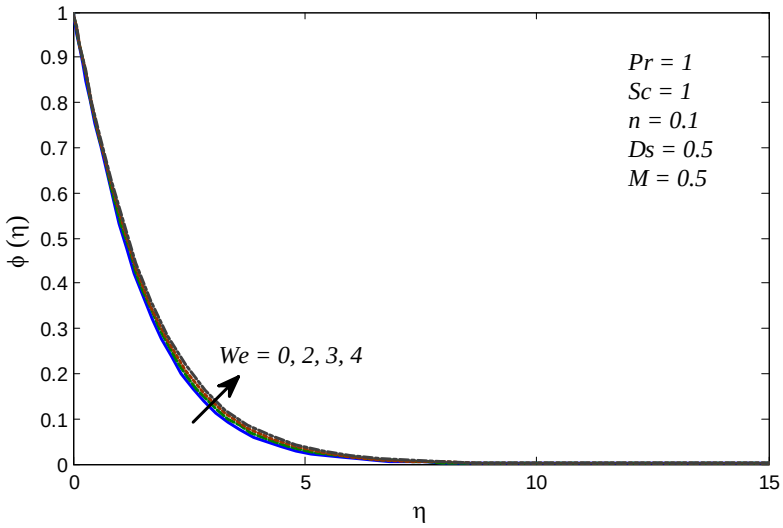

Figure 6: Graph of SRM solutions for concentration profile $\phi(\eta)$ for different values of *We*

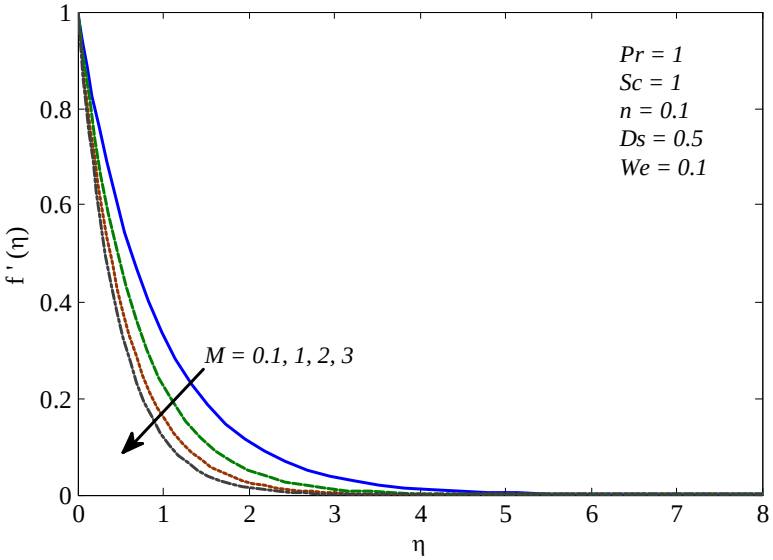

Figure 7: Graph of SRM solutions for velocity profile $f'(\eta)$ for different values of *M*

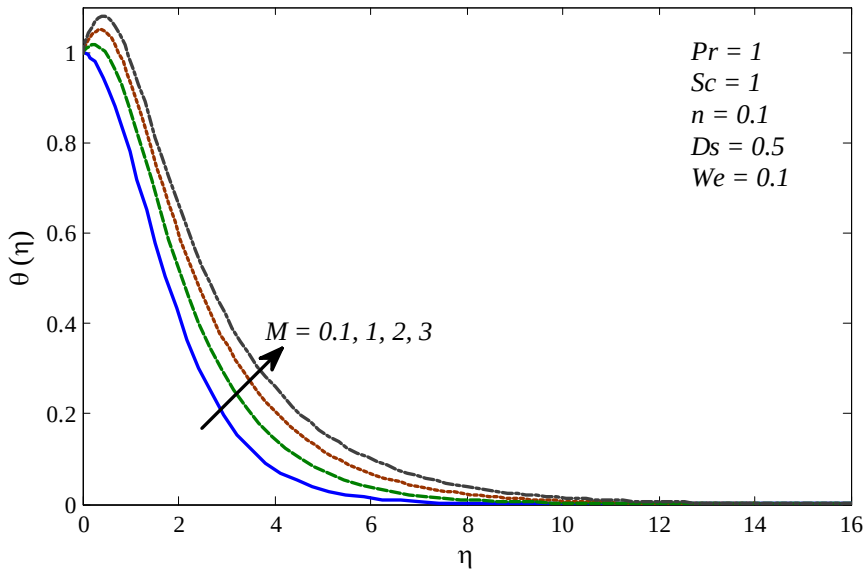

Figure 8: Graph of SRM solutions for temperature profile $\theta(\eta)$ for different values of M

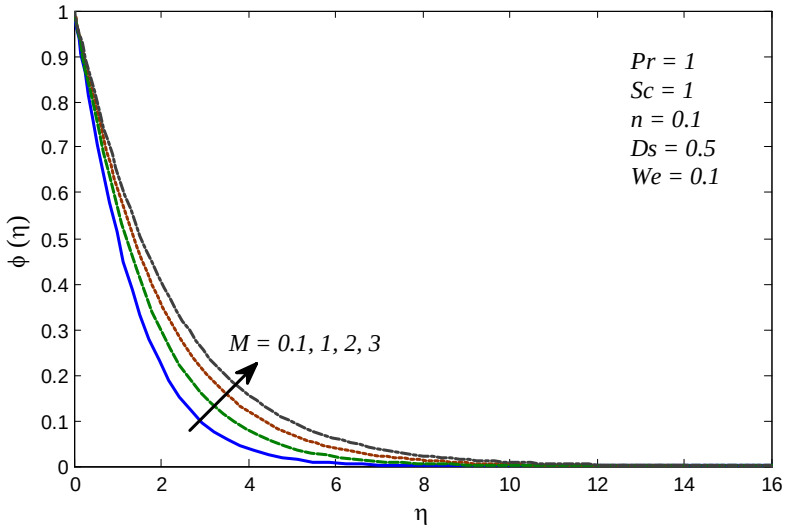

Figure 9: Graph of SRM solutions for concentration profile $\phi(\eta)$ for different values of M

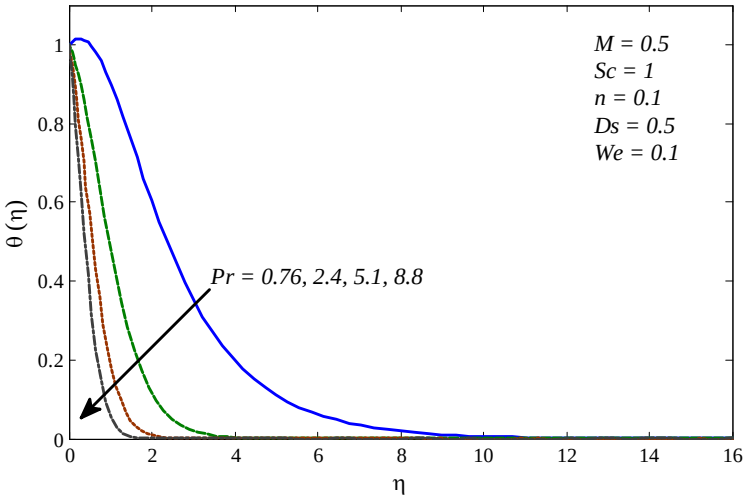

Figure 10: Graph of SRM solutions for temperature profile $\theta(\eta)$ for different values of Pr

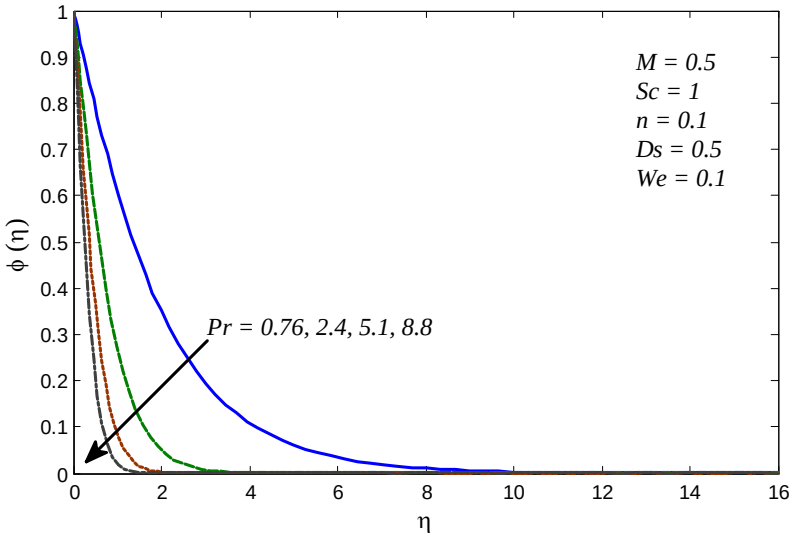

Figure 11: Graph of SRM solutions for concentration profile $\phi(\eta)$ for different values of Pr

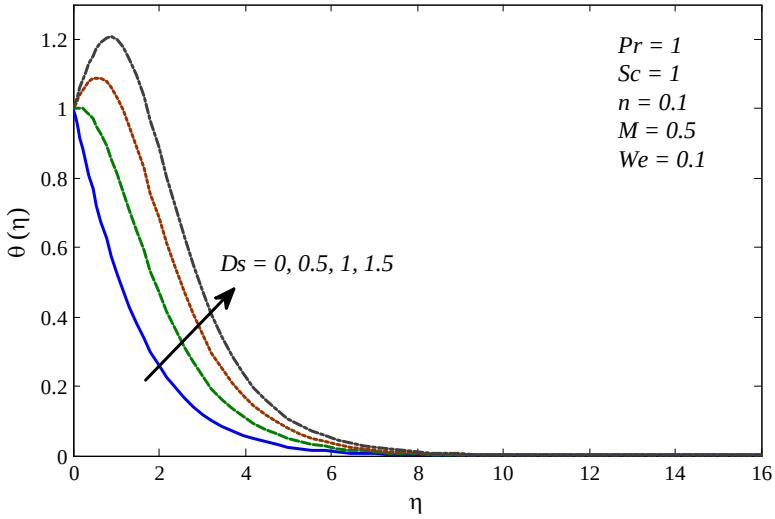

Figure 12: Graph of SRM solutions for temperature profile $\theta(\eta)$ for different values of *Ds*

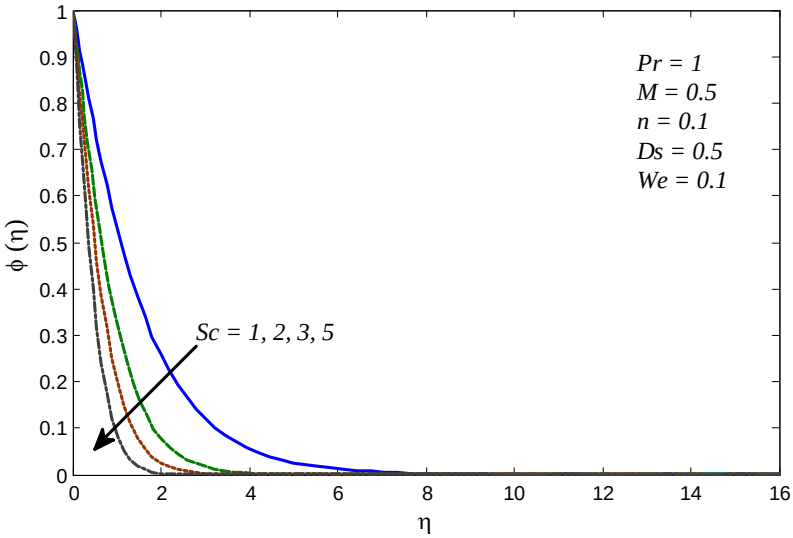

Figure 13: Graph of SRM solutions for concentration profile $\phi(\eta)$ for different values of *Sc*

Table 1 Numerical values for magnitude of $\sqrt{\mathrm{Re}_x}C_{fx}$ at the surface for different values of n, We & M with $\mathrm{Pr} = Sc = 3, Ds = 0.5..$

n	We	M	$\sqrt{\mathrm{Re}_x}C_{fx}$	
			SRM	bvp4c
0.1	0.1	0.5	1.15892610	1.15892610
0.2	0.1	0.5	1.08871946	1.08871946
0.3	0.1	0.5	1.01304949	1.01304949
0.4	0.1	0.5	0.93028371	0.93028371
0.5	0.1	0.5	0.83768770	0.83768770
0.1	0.5	0.5	1.14675023	1.14675023
0.1	1.0	0.5	1.13077992	1.13077992
0.1	1.5	0.5	1.11383010	1.11383010
0.1	2.0	0.5	1.09568709	1.09568709
0.1	0.1	1.0	1.33774497	1.33774497
0.1	0.1	1.5	1.49517344	1.49517344
0.1	0.1	2.0	1.63740820	1.63740820
0.1	0.1	2.5	1.76813004	1.76813004

Table 2 Numerical values for $-\theta'(0)$ at the surface for n, We, M, Ds & Pr for $Sc = 3$.

n	We	M	Ds	Pr	$-\theta'(0)$	
					SRM	bvp4c
0.1	0.1	0.5	0.5	3	0.34830914	0.34830914
0.2	0.1	0.5	0.5	3	0.30469477	0.30469477
0.3	0.1	0.5	0.5	3	0.25143371	0.25143371
0.4	0.1	0.5	0.5	3	0.18377463	0.18377463
0.5	0.1	0.5	0.5	3	0.09225247	0.09225247
0.1	0.5	0.5	0.5	3	0.33725987	0.33725987
0.1	1.0	0.5	0.5	3	0.32193450	0.32193450
0.1	1.5	0.5	0.5	3	0.30445542	0.30445542
0.1	2.0	0.5	0.5	3	0.28404527	0.28404527
0.1	0.1	1.0	0.5	3	0.24781975	0.24781975
0.1	0.1	1.5	0.5	3	0.16275842	0.16275842
0.1	0.1	2.0	0.5	3	0.08840660	0.08840660
0.1	0.1	2.5	0.5	3	0.02199313	0.02199313
0.1	0.1	0.5	0.6	3	0.26010269	0.26010269
0.1	0.1	0.5	0.7	3	0.18384194	0.18384194
0.1	0.1	0.5	0.9	3	0.05926624	0.05926624
0.1	0.1	0.5	1.0	3	0.00800780	0.00800780
0.1	0.1	0.5	0.5	4	0.50654478	0.50654478
0.1	0.1	0.5	0.5	5	0.64876889	0.64876889
0.1	0.1	0.5	0.5	6	0.77905057	0.77905057
0.1	0.1	0.5	0.5	7	0.89997906	0.89997906

Table 3 Numerical values for $-\phi'(0)$ at the surface for n, We, M, Pr& Sc .

n	We	M	Pr	Sc	$-\phi'(0)$	
					SRM	bvp4c
0.1	0.1	0.5	3	3	2.11379991	2.11379991
0.2	0.1	0.5	3	3	2.09506064	2.09506064
0.3	0.1	0.5	3	3	2.07181181	2.07181181
0.4	0.1	0.5	3	3	2.04183423	2.04183423
0.5	0.1	0.5	3	3	2.00093393	2.00093393
0.1	0.5	0.5	3	3	2.10941226	2.10941226
0.1	1.0	0.5	3	3	2.10342617	2.10342617
0.1	1.5	0.5	3	3	2.09676513	2.09676513
0.1	2.0	0.5	3	3	2.08925300	2.08925300

0.1	0.1	1.0	3	3	2.06974599	2.06974599
0.1	0.1	1.5	3	3	2.03088851	2.03088851
0.1	0.1	2.0	3	3	1.99576760	1.99576760
0.1	0.1	2.5	3	3	1.96351627	1.96351627
0.1	0.1	0.5	4	3	2.48458453	2.48458453
0.1	0.1	0.5	5	3	2.81118869	2.81118869
0.1	0.1	0.5	6	3	3.10641603	3.10641603
0.1	0.1	0.5	7	3	3.37787318	3.37787318
0.1	0.1	0.5	3	4	2.48458453	2.48458453
0.1	0.1	0.5	3	5	2.81118869	2.81118869
0.1	0.1	0.5	3	6	3.10641603	3.10641603
0.1	0.1	0.5	3	7	3.37787318	3.37787318

Table 4 Comparison of Skin-friction coefficient $\sqrt{\mathrm{Re}_x}C_{fx}$ with the available results in literature for different values of n & We when $\mathrm{Pr} = Sc = Ds = M = 0$.

	$\sqrt{\mathrm{Re}_x}C_{fx}$					
	$We = 0.0$		$We = 0.3$		$We = 0.5$	
n	Present study	Akbar et al. [26]	Present study	Akbar et al. [26]	Present study	Akbar et al. [26]
0.0	1.00000000	1.00000	1.00000000	1.00000	1.00000000	1.00000
0.1	0.94868330	0.94868	0.94247918	0.94248	0.93825864	0.93826
0.2	0.89442719	0.89442	0.88022646	0.88023	0.87026055	0.87026

REFERENCES

[1]. Wang, XQ, Mujumdar, AS., (2007), Heat transfer characteristics of nanofluids: a review. International Journal of Thermal Science, Vol.46, pp.1-19.

[2]. Xu H. and Jun Liao S., (2009), Laminar flow and heat transfer in the boundary-layer of non-Newtonian fluids over a stretching flat sheet, Computers & Mathematics with Applications, Vol.57(9), pp.1425-1431.

[3]. Xu H, Liao SJ, & Pop I, (2006), Series solution of unsteady boundary layer flows of non-Newtonian fluids near a forward stagnation point, Journal of Non-Newtonian Fluid Mechanics, Vol.139, pp.31–43.

[4]. Megahed A.M., (2015), Flow and heat transfer of a non-Newtonian power – law fluid over a non-linearly stretching vertical surface with heat flux and thermal radiation, Meccanica, Vol.50(7), pp.1693-1700.

[5]. Abel M.S., Datti P.S. , Mahesha N., (2009), Flow and heat transfer in a power-law fluid over a stretching sheet with variable thermal conductivity and non-uniform heat source, International Journal of Heat and Mass Transfer, Vol.52(11-12), pp.2902-2913.

[6]. Bilal Ashraf M., Hayat T., Alsaedi A., (2015), Convective heat and mass transfer in MHD mixed convection flow of Jeffrey nanofluid over a radially stretching surface with thermal radiation, Journal of Central South University, Vol.22(3), pp.1114-1123.

[7]. Wei DM, & Al-Ashhab S, (2014), Similarity solutions for non-Newtonian power-law fluid flow, Applied Mathematics and Mechanics, Vol. 35(9), pp 1155–1166.

[8]. Zheng L & Zhang XJ, (2008), On energy boundary layer equations in power law non-Newtonian fluids, Journal of Central South University of Technology, Vol.15, pp.5-8.

[9]. Wang C & Tu C, (1989), Boundary-layer flow and heat transfer of non-Newtonian fluids in porous media, International Journal of Heat and Fluid Flow, Vol.10(2), pp.160-165.

[10]. Hady FM, (1995), Mixed convection boundary-layer flow of non-Newtonian fluids on a horizontal plate, Applied Mathematics and Computation, Vol.68, pp.105-112.

[11]. Gorla RSR, (1986), Combined forced and free convection in boundary layer flow of non-Newtonian fluid on a horizontal plate, Chemical Engineering Communications, Vol.49, pp.13-22.

[12]. Mostafa AAM, (2011), Slip velocity effect on a non-Newtonian power-law fluid over a moving permeable surface with heat generation. Mathematical and Computer Madelling, Vol.54, pp.1228-1237.

[13]. Friedman AJ, Dyke SJ, & Phillips BM, (2013), Over-driven control for large-scale MR dampers, Smart Materials and Structures, Vol. 22, 045001, 15pp.

[14]. Nadeem S, Akram S, (2009), Peristaltic transport of a hyperbolic tangent fluid model in an asymmetric channel, Zeitschrift für Naturforschung A., Vol. 64a, pp.559–567.

[15]. Nadeem S, Akram S, (2010), Effects of partial slip on the peristaltic transport of a hyperbolic tangent fluid model in an asymmetric channel, International Journal for Numerical Methods in Fluids, Vol.63, pp.374–394.

[16]. Naseer M, Malik MY, Nadeem S, & Rehman A, (2014), The boundary layer flow of hyperbolic tangent fluid over a vertical exponentially stretching cylinder, Alexandria Engineering Journal, Vol. 53, pp.747–750.

[17]. Kelly, D., Vajravelu, K. and Andrews, L.(1999): Analysis of Heat and Mass Transfer of a Viscoelastic, Electrically Conducting Fluid past a Continuous Stretching Sheet, Nonlinear Analysis ,Vol. 36, No. 6, pp. 767- 784

[18]. Vajravelu K., Sreenadh S., and Saravana R., (2013), Combined influence of velocity slip, temperature and concentration jump conditions on MHD peristaltic transport of a Carreau fluid in a non-uniform channel, Applied Mathematics and Computation, Vol.225, pp.656-676.

[19]. Jayachandra Babu M., Sandeep N., (2016), MHD non-Newtonian fluid flow over a slendering stretching sheet in the presence of cross-diffusion effects, Alexandria Engineering Journal, Vol.55, pp.2193–2201.

[20]. Ferdows M. and Hamad M.A.A., (2016), MHD flow and heat transfer of a power – law non-Newtonian nanofluid (Cu-H2O) over a vertical stretching sheet, Journal of Applied Mechanics and Technical Physics, Vol.57(4), pp.603-610.

[21]. Satya Narayana P.V., Harish Babu D., (2016), Numerical study of MHD heat and mass transfer of a Jeffrey fluid over a stretching sheet with chemical reaction and thermal radiation, Journal of the Taiwan Institute of Chemical Engineers, Vol.59, pp.18–25.
[22]. Kasim A., Mohammad A.R.M., (2012), Effect of thermal stratification on MHD free convection with heat and mass transfer over an unsteady stretching surface with heat source, Hall Current and chemical reaction, International Journal of Advances in Engineering Science and Applied Mathematics, Vol.4(3), pp.217-225.
[23]. Rushi Kumar B., (2013), MHD boundary layer flow on heat and mass transfer over a stretching sheet with slip effect, Journal of Naval Architecture and Marine Engineering, Vol. 10, pp.16-26.
[24]. Pal D., Mandal G., and Vajravelu K., (2016), Soret and Dufour effects on MHD convective-radiative heat and mass transfer of nanofluids over a vertical non-linear stretching/shrinking sheet, Applied Mathematics and Computations, Vol.287, pp.184-200.
[25]. Kumari M & Nath G, (2001), MHD boundary layer flow of a non-Newtonian fluid over a continuously moving surface with a parallel free stream, Acta Mechanica, Vol.146(3), pp 139–150.
[26]. Akbar NS, Nadeem S, Haq RU and Khan ZH, (2013), Numerical solutions of Magnetohydrodynamic boundary layer flow of tangent hyperbolic fluid towards a stretching sheet, Indian Journal of Physics, Vol.87(11), pp.1121–1124.
[27]. Salahuddin T, Malik MY, Hussain A, Bilal S, & Awais M, (2015), Effects of transverse magnetic field with variable thermal conductivity on tangent hyperbolic fluid with exponentially varying viscosity, AIP Advances, Vol.5, 127103.
[28]. Bear J., (1972), Dynamics of Fluids in Porous Media, Dover Publications.
[29]. Georgiadis J.G., Catton I., (1988), Dispersion in cellular convection in porous layers, International Journal of Heat and Mass Transfer, Vol. 31, pp.1081–1091.
[30]. Hong J.T., Tien C.L., (1987), Analysis of thermal dispersion effect on vertical plate natural convection in porous media, International Journal of Heat and Mass Transfer, Vol. 30, pp.143–150.
[31]. El-Amin M.F., Aissa W.A., Salama A., (2008), Effect of chemical reaction and double dispersion on non-Darcy free convection heat and mass transfer, Transfer in Porous Media, Vol.75, pp.93-109.
[32]. Motsa S.S. and Makukula Z.G., (2013), On spectral relaxation method approach for steady von kárman flow of a reiner-rivlin fluid with joule heating, viscous dissipation and suction/injection. Central European Journal of Physics, Vol.11(3), pp.363–374.
[33]. Kameswaran P, Sibanda P, and Motsa SS, (2013). A spectral relaxation method for thermal dispersion and radiation effects in a nanofluid flow. Boundary Value Problems 2013, 242.